Zeitschrift für Anorganische und Allgemeine Chemie

A Spectroscopic and Structural Study of M(3d)2+ – Doped β-Tricalcium Phosphate – the Binding Properties of Ni2+ and Cu2+ in the Pseudo-octahedral Ca(5)O 6 Host-Sites.

Journal:	*Zeitschrift für Anorganische und Allgemeine Chemie*
Manuscript ID:	zaac.200900236
Wiley - Manuscript type:	Article
Date Submitted by the Author:	22-Apr-2009
Complete List of Authors:	Mayer, Isaac; Hebrew University, Department of Chemistry Gdalya, Sarit; Hebrew University, Department of Chemistry Burghaus, Olaf; Philipps-Universität Marburg, Fachbereich Chemie Reinen, Dirk; Philipps-Universität Marburg, Fachbereich Chemie
Keywords:	nickel, Copper, calcium phosphate

A Spectroscopic and Structural Study of $M(3d)^{2+}$ – Doped β-Tricalcium Phosphate – the Binding Properties of Ni^{2+} and Cu^{2+} in the Pseudo-octahedral $Ca(5)O_6$ Host-Sites.

Isaac Mayer[a], Sarit Gdalya[a], Olaf Burghaus[b] and Dirk Reinen[b]*

Keywords: Nickel(II) and Copper(II). β-Tricalcium Phosphate, the $Ca(5)^{2+}$ Site. d-d Absorption and EPR Spectra.

Abstract
The pseudo-octahedral $Ca(5)^{2+}$ position in β-$Ca_3(PO_4)_2$ is a higly interesting host site with unexpectedly short Ca-O bond lengths, which can be easily substituted by small 3d-cations, such as Ni^{2+}. Also Cu^{2+} may fully replace $Ca(5)^{2+}$, leading to remarkably large energetic and steric distortion effects due to $E_g \otimes \varepsilon_g$ Jahn-Teller coupling – with a ground state splitting of about 1.25 eV. The Cu(Ni)-O bond is strongly ionic according to a 3d-mixing coefficient of the e_g-electrons around 0.90, as revealed by EPR- and d-d spectroscopy. It is suggested, that the flexibility of the $Ca(5)O_6$ host polyhedra, which lie isolated in the lattice, in respect to deformations and to substitutions by smaller cations is one reason for the practicability of β-TCP as a biocompatible material.

* Prof. Dr. D. Reinen
E-Mail: reinen@chemie.uni-marburg.de
[a] Department of Inorganic and Analytical Chemistry
Hebrew University
Jerusalem 91904, Israel
[b] Fachbereich Chemie
Philipps Universität
35032 Marburg, Germany

I. Introduction

β-Tricalcium phosphate (β-TCP) crystallizes in the rhombohedral space group R3c and is isomorphous with the mineral Whitlockit [1]. The solid is an important biomaterial, widely used in implants. It was recently shown [2], that Mn^{2+} ions can fully substitute Ca^{2+} in the Ca(5) position, according to the constitution $Ca_{2.71}Mn_{0.29}(PO_4)_2$. The latter site is pseudo-octahedral and shows unusually small Ca-O bond lengths of a=2.26_5(2_5) Å as compared to that in CaO (2.40_5 Å). Apparently, a considerable intra-lattice strain is enforced upon the $Ca(5)O_6$ polyhedra – which lie isolated from each other in the structure – by their environment. If half of the $Ca(5)^{2+}$ cations is substituted by Mn^{2+}, a further decrease of the bond lengths by about 0.15 Å is observed – more than expected from ionic radii [3] considerations. Even the distinctly smaller Mg^{2+} cation can fully occupy the Ca(5) position, with reported Mg-O bond lengths of 2.07_5 Å [4]; here, the latter are not too far from those in MgO (2.10_5 Å). Thus, one might suppose that Ni^{2+}, with an only slightly smaller ionic size, could be incorporated into Ca(5) sites as well and should be also largely released from the - for larger cations - anticipated intra-lattice strain. The same should hold for Cu^{2+} with an equally comparable ionic radius; here, the steric modelling of the host polyhedron, induced by the pronounced Jahn-Teller coupling, is an additionally interesting feature.

II. Sample characterisation.

a) Preparation and X-ray diffraction analysis

The synthesis of Ni^{2+}-containing hydroxyapatite was performed by dropping a phosphate solution [3.7 g $(NH_4)_2HPO_4$ in 200 ml triple distilled water TDW] to a calcium solution [9.47 g $Ca(NO_3)_2.4H_2O$ in 200 ml TDW] during 2h and constant stirring. Ni^{2+} was added from a $Ni(NO_3)_2$ solution. The pH of preparation was 7.0 and maintained constant during precipitation via a pH-stat adding NaOH solution. The precipitation was carried out at 85ºC, before the temperature was raised to the boiling point, and the system refluxed for further 2h. The sample is then washed with TDW and dried overnight in air at 120ºC. The X-ray powder diffraction pattern contained only reflections characteristic for the P6/3 hexagonal structure of hydroxyapatites [5a], without any additional impurity lines.
The synthesis of Ni^{2+}- and Cu^{2+}-containing ß-TCP, with the compositions $Ca_{2.8}Ni_{0.2}(PO_4)_2$ and $Ca_{2.85}Cu_{0.15}(PO_4)_2$, was performed by high temperature solid-state reaction, using a stoichiometric mixture of $CaCO_3$, $(NH_4)_2HPO_4$ and $Ni(Cu)(NO_3)_2$. The latter was homogenized in an agate mortar, heated in an alumina crucible at 300ºC for three hours, crushed, mortared again and heated at 1100ºC overnight. The crystal phase of the samples was determined by powder X-ray diffraction with a Philips Automatic Diffractometer, using CuKα radiation. The samples were scanned in the 2θ range of 20-55º. The lattice parameters were calculated by a least-square computer program, with a maximum deviation of ±0.003Å. The compounds crystallize in the R3c rhombohedral structure characteristic of ß-TCP [5b]. No reflections of impurity phases were present. The lattice constants: a=10.36 Å; c=37.20 Å, in the case of $Ca_{2.8}Ni_{0.2}(PO_4)_2$, and a=10.38 Å; c=37.30 Å, in the case of $Ca_{2.85}Cu_{0.15}(PO_4)_2$, are smaller than those known for $Ca_3(PO_4)_2$, indeed indicating the partial substitution of Ca^{2+} by the smaller Ni^{2+} and Cu^{2+} ions. Small

single crystals of the constitution ß–$Ca_{2.82}Ni_{0.18}(PO_4)_2$ were obtained, when slowly cooling the reaction mixture from 1100ºC to ambient temperature. Details of the structure determination are reported elsewhere [6]. The calculated P^V–O and Ca^{II}–O bond lengths, with the exception of those in the $Ca(5)O_6$ polyhedron, where the substitution occurs, are identical within the error-limit with those, reported in ref. [2] for P^V–O, while the average Ca(i)–O[i=1-4] bond lengths differ from the ones in $Ca_{2.85}Mn_{0.15}(PO_4)_2$ [2] by less than +0.01 Å in the utmost. The bond lengths and bond angles in the pseudo-octahedral $Ca(5)O_6$ polyhedron, in comparison to various other structural data for β-TCP with a partial substitution of Ca^{2+} by Mg^{2+} and Mn^{2+}, are collected in Table 1. The listed structural results indeed provide evidence for the anticipated intra-lattice strain on particularly the $Ca(5)O_6$ polyhedron. If large cations occupy the site, the respective octahedra are considerably compressed, yielding bond lengths, which are smaller by about 0.15 Å with respect to those, expected from ionic radii considerations (see also the Introduction). If however, smaller cations, such as Ni^{2+} and Mg^{2+}, are inserted, the structural situation has largely normalized; here, the latter cations seem to create that space, which they usually take advantage of. Because furthermore the $M(5)^{II}O_6$ polyhedra lie isolated from each other in the lattice, rather normal binding properties for Ni^{2+} – but also for Cu^{2+} – in the $M(5)^{2+}$ site can hence be anticipated. In the d^9 case the trigonal distortion of the host polyhedron is expected to modify the vibronic Jahn-Teller coupling significantly and accordingly to give further informations about the properties of the $Ca(5)^{2+}$ site in the biomaterial; there, EPR spectroscopy is the probe-method of choice. We mention finally that the structural data in Table 1 seem to indicate, that the trigonal bond length differences– but not significantly the angular distortion of the $M(5)^{II}O_6$ polyhedra – become smaller with diminishing average bond length.

b) The spectroscopic investigation.

IR-Vis spectra between 5000 and 28000 cm^{-1} were recorded at 298 K, using the powder-reflection technique (Zeiss PMQII and Hitachi U-3410).
Electron Paramagnetic Resonance (EPR) spectra were recorded on a Bruker ESP300 spectrometer with a Varian TE102 rectangular cavity and 25 kHz field modulation. The spectometer is equipped with an Oxford Instruments ESR 900 helium flow cryostat. EPR parameters were extracted using the fit and simulation program SIMEPR [7].

III. Results and Discussion

a) Nickel (II)

Figure 1 shows the well-resolved d-d spectrum of β-$Ca_3(PO_4)_2$, in which a little less than 7 molar percent of the Ca^{2+} cations are substituted by Ni^{2+}. The band energies can be nicely reproduced by the two-parameter set in Table 2, using the master equations in ref. [8] and the free ion ratio of 4.2 between the Racah parameters of interelectronic repulsion C and B. Even the spin forbidden transitions $^3A_{2g} \rightarrow {}^1_a E_g$, ${}^1_a T_{2g}$ are seen.The $^3A_{2g} \rightarrow {}^3_a T_{1g}$ transition is broadened due to spin-orbit coupling. We cannot account for the distinct band at 18800 cm^{-1}, which is possibly caused by a tiny Ni^{2+} percentage on one of the other Ca^{2+} sites in the β-TCP structure with considerably larger Ca-O distances than the ones in Ca(5). It is assigned to $^3A_{2g} \rightarrow$

$^3_bT_{1g}$ with an accordingly very small Δ parameter – not unusual for a substitution into voluminous Ca^{2+} positions [9]; the other two spin-allowed d-d transitions vanish under the first main band of Ni^{2+} in the Ca(5) site ($\rightarrow$ $^3_aT_{1g}$) and appear only outside the reliably accessible range of measurement < 5000 cm^{-1} ($\rightarrow ^3T_{2g}$), respectively (Fig.1). The yellow hue is due to the colour-determining minimum in the visible region between 15 and 20000 cm^{-1}. The nephelauxetic ratio $\beta = B/B_o$, which measures the decrease of the interelectronic repulsion in respect to to the value of the free ion (B_o = 1040 cm^{-1}), is near to 0.9, indicating a rather ionic Ni-O bond (Table 2). This can be led back to the strong contrapolarizing power of P^V, to which the oxygen ligator atom is bonded [9]. It enhances the oxygen electronegativity and hence the tendency to form ionic bonds (see also other solids with PO_4^{3-}-type ligands in Table 2). Even stronger is the polarizing strength of protons on oxygen and somewhat less the one of the C^{IV} atom, while in NiO the oxygen ligand is more covalent. The variation of the ligand field strength Δ is more complex to interpret, because it also strongly depends on the interplay between σ- and π-overlap [9].

Fig.2 shows the spectrum of an, in the presence of carbonate, precipitated hydroxyapatite (HA) sample HANi1 with less than 1% Ni^{2+}. Though the spectrum is broad, Δ and B could be well determined. The β ratio suggests a comparatively ionic Ni-O bond, and – together with the larger Δ value – indicates, that Ni^{2+} is apparently mainly bonded to hydroxo-groups. A distinctly smaller Δ-parameter is expected, if Ni^{2+} would enter one of the large Ca^{2+} sites in the apatite lattice. A binding of Ni^{2+} to CO_3^{2-} can be also discarded because a considerably larger ligand field parameter should result in such a case (Table 2). The second spectrum in Fig.2 stems from an HA sample with 1,2% Ni^{2+} (HANi2) precipitated from solution, but, in difference to the sample considered before, without carbonate presence. The position of the first transition is obscured by an overtone mode of H_2O at 7200 cm^{-1}, the even more intense absorption at 5200 $cm^{-1}$is also due to water (combination-type mode). The by nearly 15% smaller Δ value as compared to that for HANi1 suggests, that Ni^{2+} is bonded to phosphate groups solely (Table 2). Heating to 800ºC leads to grayish colours in both cases and indicates – though the bulk sample has undergone a phase transition to β-TCP at this temperature – that nickel is present in an impurity phase. Only at higher temperatures the metal enters the β-TCP structure as Ni^{2+} and a pure (slightly blue-shifted) yellowish colour reappears.

After all optical spectra provide some insight into the formation mechanism of the Ni-containing bulk and impurity phases.

b. Copper (II)

Fig.3 shows the d-d spectra of two different samples with the constitution $Ca_{2.71}Cu_{0.29}(PO_4)_2$ and the β-$Ca_3(PO_4)_2$ structure. The blue colour of the pure Cu^{II} compound is caused by the deep minimum between 20 and $25 \cdot 10^3$ cm^{-1}, which appears after the well resolved d-d transitions of the $Cu^{II}O_6$ polyhedron on the trigonal $Ca(5)O_6$ position. Depending on the preparation procedure also grayish colours may be observed, which are caused by traces of Cu^{III}; they obscure the spectrum by giving rise to a lower-energy shift of charge-transfer absorptions, which in particular fill the mentioned minimum. The assignment of the d-d bands is straightforward and reveals a distinct orthorhombic symmetry component. The usually broad and weak transition within the octahedral $^2E_g(t_{2g}^6\ e_g^3)$ parent state is indicated as a shoulder upon the lower-energy ascent toward the split states of the excited octahedral $^2T_{2g}$ parent state

and is coarsely estimated via band shape analysis to occur at 10(±1) 10^3 cm^{-1}. This splitting is unexpectedly large and reveals a vibronic Jahn-Teller coupling of considerable strength [11]. The magnitude of the octahedral ligand field parameter is approximated from the centres of gravity of the $^2_aA_g$, $^2_bA_g(^2E_g)$ and $^2B_{1g}$, $^2B_{2g}$, $^2B_{3g}$ ($^2T_{2g}$) states, respectively, to $\Delta_0 = 8.5(5)\cdot10^3$ cm^{-1} – not too far from the values for Ni^{2+} in the same or similar host structures (Table 2). This finding confirms our assignment.

EPR spectroscopy provides further and more detailed informations about the binding situation of Cu^{2+} in the Ca(5) site of β-TCP. While at larger concentrations a sharp isotropic signal appears between 4 and 300K – exchange-narrowed due to interactions between neighboured Cu^{2+} centers in the lattice ($g_{ex} \approx 2.20$) – at a low doping level and at low temperatures resolution into a strongly anisotropic signal of approximately tetragonal shape occurs (Fig. 4). Though the hyperfine splitting in the $g_{\|}(=g_z)$ signal due to the electron (S = 1/2)-nucleus (I = 3/2) interaction is well resolved, only rather indistinct signal anisotropies are recognizable in the region of $g_\perp$. The resolution is perceptibly enhanced in the second-derivative spectrum, which reveals both, the orthorhombic symmetry component and a small, but significant difference in the hyperfine splitting of g_y and g_x (Fig. 5); the spectral parameters, obtained by simulation of the experimental spectrum, are listed in Table 3. Fig. 5 shows also, that the simulation is just partly successful in the region of 320 mT. The reason is disclosed, when inspecting the temperature dependence in Fig. 6. At ≥ 150 K the Cu^{2+} signals disappear, leaving an impurity signal at the above location as the only spectral feature. The EPR spectra at Q band frequency supplement the X-band results (Fig. 7, bottom and top, respectively). They nicely mirror the transition from the statically distorted CuO_6 polyhedron to the thermally averaged regular octahedron via the anisotropic spectrum at ≤ 7K and the broad isotropic signal at an averaged g-value of $g_{av}\approx2.22$ at ambient temperature. Also here the impurity signal appears at the expected position.

The $^2_aA_g$ ground state wave function of the unpaired e_g-electron of Cu^{2+} in an orthorhombically distorted octahedral ligand field is:

$$\psi_g = (\cos\varphi/2)\, d_{x2-y2} + (\sin\varphi/2) d_{z2} \qquad (1)$$

The second term takes account of an admixture of d_{z^2} to the $d_{x^2-y^2}$ ground state, which is possible in D_{2h} for symmetry reasons. The deviations of the g- values from the spin-only value 2.0023 can be shown to obey the following expressions [12]:

$$\delta g_x = 4u_z\,(1+\cos\varphi) \qquad (2)$$

$$\delta g_y = 2u_y(2 + \sqrt{3}\sin\varphi - \cos\varphi)$$

$$\delta g_z = 2u_x\,(2 - \sqrt{3}\sin\varphi - \cos\varphi)$$

The $u_i(i = z,y,z)$ are the orbital contributions to the g-tensor components:

$$u_i = k_i^2\xi_o/\Delta E_i;$$
$$\Delta E_i = E(^2_aA_g \rightarrow {}^2B_{1g}[z], {}^2B_{2g}[y], {}^2B_{3g}[x]) \qquad (2a)$$

and the ΔE_i the transition energies from Fig. 3. The k_i constitute the orbital reduction factors, which reduce the magnitude of the L-S coupling constant with respect to the value for the free Cu^{2+} cation (ξ_0 = 830 cm^{-1}); they are defined via the electron delocalisation within the relevant σ-and π-antibonding MOs, originating from d_{x2-y2} (d_{z2}) and d_{xy}, d_{xz}, d_{yz}, respectively:

$$^2_a A_g : \quad \Phi_g = c_1\psi_g - c_1'L_g \qquad (3)$$

$$^2B_{1g} : \quad \Phi_3 = c_3 d_{xy} - c_3'L_{xy}$$

$$^2B_{2g} : \quad \Phi_4 = c_4 d_{xz} - c_4'L_{xz}$$

$$^2B_{3g} : \quad \Phi_5 = c_5 d_{yz} - c_5'L_{yz}$$

The L_j (j = g, xy, xz, yz) are symmetry-adapted combinations of ligand orbitals, and the k_i factors correlate with the involved mixing coefficients c_i via the relations:

$$k_z = c_1.c_3 \qquad k_y = c_1.c_4 \qquad k_x = c_1.c_5 \qquad (3a)$$

The latter are expected to be near to unity in the case of π-antibonding, particularly if large bond lengths are involved ($c_3 \leq c_4 \approx c_5 \leq 1$). The estimation of the k_z and $k_x \approx k_y$ reduction factors and of the angular parameter φ from the experimental g_i tensor components (Table 3) is now straightforward, utilizing eqs (2) and the d-d transition energies ΔE_i from Fig. 3. The obtained k_i (Table 3) mainly reflect the mixing coefficient c_1 in the σ-antibonding $^2_a A_g$ ground state (eqs (3)); from these values, and with the rough assumption $c_4 = c_5 \approx 1.0$, one estimates: $c_1 \approx 0.92$ (see below). The derived φ = 6.5° signalises a significant deviation from D_{4h} (φ = 0°), with an about 6% d_{z^2}-admixture to the ground state (eq. (1)). The bond length-differences Δa_i (i= x,y,z) from the average metal-ligand distance a_{av} in the CuO_6 polyhedron define the radial distortion parameter:

$$\rho = \{2\,(\Delta a_x^2 + \Delta a_y^2 + \Delta a_z^2)\}^{½} \qquad (4)$$

The angular parameter φ specifies the relative magnitudes of the Δa_i:

$$\Delta a_z/\rho = (1/\sqrt{3})\cos\varphi \qquad (5)$$

$$\Delta a_{y(x)}/\rho = (1/2\sqrt{3})(-\cos\varphi + (-)\sqrt{3}\sin\varphi)$$

Utilizing a ρ-value 0.5 Å and an average bond length of 2.1 Å , one obtains (with the experimental angular distortion φ) the bond lengths within the CuO_6 polyhedron, listed in Table 3. The chosen structural parameters are near to those [13] , derived for the expasolites Ba_2CuWO_6 and $Sr_2CuW(Te)O_6$, where the d-d spectra yield a ground splitting of about 8500 cm^{-1}, not too far from the one observed here. The polyhedron orthorhombicity, evident in the d-d spectra and in EPR, is the – by symmetry enforced – consequence of the vibronic Jahn-Teller coupling which demands an elongated D_{4h} distortion, but has to take account of the trigonally-shaped host site as well. One

derives from eq. (5), that φ = 60º (-60º) corresponds to an, along the molecular x(y) axis tetragonally compressed octahedron, while the intermediate angles φ = 30º, -30º refer to polyhedron distortions of extreme orthorhombicity.

More fundamental information about the binding within the CuO_6 polyhedron may be drawn from the EPR hyperfine constants, which are available from the simulation in Fig. 5 (Table 3). The magnetic hyperfine interaction between the copper nucleus and the unpaired electron gives rise to the following magnitudes of the A_i tensor components [12, 14]:

$$A_z/ P = c_1^2[-\kappa - 4/7 \cos \varphi] + \delta g_z + 1/14\{(3 + 2\sqrt{3}\sin \varphi)\, \delta g_x + (3-2\sqrt{3}\sin \varphi)\, \delta g_y \}/(2\cos \varphi - 1) \quad (6)$$

$$A_{y(x)}/P = c_1^2[-\kappa + 2/7(\cos \varphi -(+) \sqrt{3}\sin \varphi)] + \delta g_{y(x)} +(-) \sqrt{3}/14\{\sin \varphi /(\cos\varphi+1)\}\, \delta g_z -1/14\{(3 +(-) 2\sqrt{3}\sin \varphi)/(2\cos \varphi-1)\}\, \delta g_{x(y)}$$

$$A_{av)}/P \equiv 1/3 \sum_i A_i /P = - c_1^2\, \kappa + 1/3(\delta g_z + \delta g_y + \delta g_x) \quad (6a)$$

P is a scaling factor and calculated to amount to $360 \cdot 10^{-4}$ cm^{-1} for Cu^{2+}; κ mirrors the isotropic hyperfine contribution to the A_i, due to unpaired electron density in s-orbitals, and is 0.43 for Cu^{2+}, if polarization exclusively is the responsible interaction mechanism [15]. If, however, a direct flow of d-electron density into the s-orbitals – allowed by symmetry – occurs, a large negative contribution to κ may arise. Such an effect is expected here, because of the d_{z^2} participation in the ground state (eq 1); in the case of a tetragonal compression, and hence of a pure d_z^2 ground state, κ can be reduced to values near to zero [16]. The fitting of the experimental hyperfine tensor components A_z and A_y to eqs (6), utilizing the already derived φ-value, yields only applicable results with the choice $A_z < 0$ and $A_y > 0$. The mixing coefficient c_1 is consistent in magnitude with the k_i obtained before; the isotropic hyperfine increment κ comes out to be significantly reduced in respect to 0.43, as anticipated (Table 3). A_x, finally, is calculated to be of the magnitude $+37 \cdot 10^{-4}$ $cm^{-1.}$ – indeed very near to the fit-value (Table 3) and in spite of a possible falsification caused by the partial overlap of the g_x with the impurity signal.

IV. Summarizing remarks

The result in Tables 1-3 indicate, that a substitution of Ca^{2+} in the Ca(5) site of β-TCP by considerably smaller cation, such as Cu^{2+} and Ni^{2+}, is easily feasible. In contrast, the doping of such cations into the Ca^{2+} sites of hydroxo-apatites is not possible to a noticeable extent. Our findings confirm an earlier report[1], which claims that Mg^{2+} has a stabilizing influence on the β-TCP structure. We propose, and we have presented evidence for this, that the presence of an intra-latice strain – specifically a pressure onto the $Ca(5)O_6$ polyhedra – is the reason; the strain is only largely relieved when replacing $Ca(5)^{2+}$ by distinctly smaller divalent cations. Cu^{2+}, with a strongly Jahn-Teller unstable ground state, can be also introduced into the mentioned host site, and may even substitute $Ca(5)^{2+}$entirely. The d-d and EPR spectra mirror energetic and steric vibronic coupling effects of considerable extent in that case and suggest host polyhedra with remarkable structural flexibility. Probably, the before-mentioned

properties, in particular the practicability of an easy substitution of $Ca(5)^{2+}$ by various smaller divalent cations, are one source of the biocompability of this material in implants.

Figure 1

d-d spectrum of β-$Ca_{2.8}Ni_{0.2}(PO_4)_2$ with Ni^{2+} on the Ca(5) position; the band at 18800 cm^{-1} is presumably due to the $^3A_{2g} \rightarrow {}^3_bT_{1g}$ transition of Ni^{2+} in one of the large Ca^{2+} sites (with Δ = 4300 cm^{-1}; B = 900 cm^{-1}: $^3A_{2g} \rightarrow {}^3T_{2g}$, ${}^3_aT_{1g}$ at 4300 cm^{-1}, 7450 cm^{-1}).

Figure 2

d-d spectra of Ni^{2+} in precipitated HA, bonded to OH^- and possibly to phosphate groups (sample HANi1), and bonded to phosphate ligands solely (sample HANi2), bottom and top, respectively. Assignment with the parameters in Table 2.

Figure 3

The d-d spectra of two samples β-$Ca_{2-x}Cu_x(PO_4)_2$ with x near to 0.3, with a blue and grayish hue (see the text). The assignment is according to an orthorhombically distorted $Cu^{II}O_6$ polyhedron with an ${}^2_aA_{2g}$ ground state in D_{2h}; the tetragonal elongation predominates. The observed transition energies are: 10(1) shoulder (see the text), 11.2, 14.7 and 16.5·10^3 cm^{-1}.

Figure 4

The X-band spectrum of Cu^{2+} -doped β-TCP (1 mole% in the Ca^{2+} position) at 3K and 9.22 GHz; the inset depicts exchange narrowing at higher doping levels.

Figure 5

The second derivative of the spectrum in Fig. 4, together with the simulation; the fitting parameters are listed in Table 3.

Figure 6

The temperature dependence of the second derivative spectrum in Fig 5.

Figure 7

The temperature dependence of the EPR spectrum of Cu^{2+}-doped β-TCP at (A) 9.22 GHz, and (B) 34.00 GHz, the impurity * appears at ≈ 1.2 Tesla.

Table1. Bond lengths and bond angles within the $M^{II}(5)O_6$ polyhedron in ß-TCP: $Ca(1\text{-}4)_{2.71}Ca(5)_{0.29}(PO_4)_2$, where $Ca(5)^{2+}$ is substituted by various amounts of Mn^{2+}, Mg^{2+}, and Ni^{2+}; a_{av} is the averaged bond length and a_{ir} the one estimated from ionic radii [3].

$M(5)^{II}$	$Ca_{0.29}$	$Ca_{0.14}Mn_{0.15}$	$Ca_{0.18}Mg_{0.11}$	$Mg_{0.29}$	$Ca_{0.11}Ni_{0.18}$
M^{II}-O(4) [3x]	2.238 Å	2.088 Å	2.163 Å	2.070 Å	2.131 Å

M^{II}-O(7) [3x]	2.287 Å	2.124 Å	2.206 Å	2.084 Å	2.133 Å
O(4)-M^{II}-O(4) [3x]	82.7°	84.3°	83.7°	85.4°	83.5°
O(7)-M^{II}-O(4) [3x]	77.1°	80.2°	78.6°	79.1°	80.0°
ref.	[1]	[2]	[4]	[4]	[6]
a_{av}	2.263 Å	2.106 Å	2.185 Å	2.077 Å	2.132 Å
a_{ir} [a]	2.38 Å	2.28_7 Å	2.27_4 Å	2.10 Å	2.19_4 Å
δa [b]	-0.12 Å	-0.18 Å	-0.09 Å	-0.02 Å	-0.06 Å

a) bond lengths from ionic radii [3] – with $r(O^{2-})=1.38$ Å, valid for oxygen ligator involved in a four-coordination toward other cations (here P^V).

b) $\delta a= a_{av}-a_{ir}$.

Table 2. Ligand field parameters (in 10^3 cm^{-1}) and nephelauxetic ratios of Ni^{2+} in an octahedral oxygen environment of various solids.

Compound	Δ	B	β	colour
β -$Ca_{2.8}Ni_{0.2}(PO_4)_2$	7.65	0.92_5	0.89	greenish yellow
$LiNiPO_4$ [9]	7.90	0.92	0.88_5	greenish yellow
$Ni(PO_2Cl_2)_2(OPCl_3)_2$ [10]	7.00	0.93	0.88_5	yellow
$Ni(OH_2)_6^{2+}$ [a]	8.65	0.94_5	0.91	green
$NiCO_3$ [9]	9.20	0.89	0.85_5	bluish green
NiO [8]	8.65	0.86_5	0.83	green
HANi1 [b]	8.20	0.93	0.89_5	faint green, yellow
HANi2 [b]	≈ 7.1	0.91	0.88	faint yellow

[a] in $NiMe^{IV}F_6{\cdot}6H_2O$(Me^{IV}: Ge,Sn; Ti-Hf) [b] see text

Table 3. EPR parameters for the $Cu^{II}O_6$ polyhedron in the β-TCP host structure, derived from the spectral simulation in Fig. 5 (hyperfine constants A_i – for Cu^{63}, in 10^{-4} cm^{-1}; Lorentzian line width ΔH in Gauss; 1G ≡ 0.1 m Tesla); calculated (via eqs. (2-5) structural and binding parameters as well as estimated bond lengths (in Å) are also listed.

$g_z = 2.49_3$	$g_y = 2.11_8$	$g_x = 2.07_1$
$A_z = \lvert 77 \rvert$ [a]	$A_y = \lvert 23 \rvert$ [a]	$A_x = \lvert 40 \rvert$ [a, b]
$\Delta H_z = 44$	$\Delta H_y = 62$	$\Delta H_x= 64$
$k_z = 0.91$	$k_{xy} = 0.92$	$c_1 = 0.94$
$\varphi = 6.5°$	$\kappa = 0.27$	
$a_z \approx 2.38$ [c]	$a_y \approx 1.99$ [c]	$a_x \approx 1.93$ [c]

[a] Fitting procedure: $A_z < 0$; A_y, $A_x > 0$. [b] Calculated value: +37 (see text). [c] With $\rho = 0.5$ and $a_{av} = 2.1$ Å

References

1. B. Dickens, L.W. Schroeder, W.E. Brown, *J. Solid State Chem.* **1974**, *10*, 232.
2. I. Mayer, S. Cohen, S. Gedalya, O. Burghaus, D. Reinen, *Mater. Res. Bull.* **2008**, *43*, 447.
3. R.D. Shannon, C.T. Prewitt, *Acta Cryst.* **1969**, *B25*, 925.
4. L.W. Schroeder, B. Dickens, W.E. Brown, *J. Solid State Chem.* **1977**, *22*, 253.

5a. International Centre for Diffraction Data. Powder Diffraction File **2005,** 09-432.
5b. International Centre for Diffraction Data. Powder Diffraction File **2005**, 09-0169.
6. I. Mayer, S. Gedalya, *Acta Crystallogr.,* to be published.
7. O. Burghaus, Universität Marburg.
8. D. Reinen**,** *Ber. Bunseng. Physik. Chemie* **1965**, *69*, 82.
9. D. Reinen, M. Atanasov, Show-Ling Lee, *Coord. Chem. Rev.* **1998**, *175*, 91.
10. A. Saavedra, D. Reinen, *Z. anorg. allg. Chem.* **1977**, *435*, 91.
11. D. Reinen, C. Friebel, *Struct. Bonding* **1979**, *37*, 1.
12. A. Abragam, B. Bleany: *Electron Parmagnetic Resonance of Transition Ions***,** Clarendon Press, Oxford **1970**.
13. D. Reinen, H. Weitzel, *Z. anorg. allg. Chem.* **1976**, *424*, 31.
14. J.H. Ammeter, Thesis **1969**, ETH, Zurich, using modified equations of B.R. McGarvey in: *Trans. Metal Chem.*, Vol. 3 **1966**, 90; Marcel Dekker, New York.
15. B.N. Figgis, M.A. Hitchman*: Ligand Field Theory and its Applications***,** Wiley-Vch, **2000**.
16. G. Steffen, D. Reinen, H. Stratemeier, M.J. Riley, M.A. Hitchman, H.E. Matthies, K. Recker, F. Wallrafen, J.R. Niklas, *Inorg Chem***. 1990**, *29*, 2123.

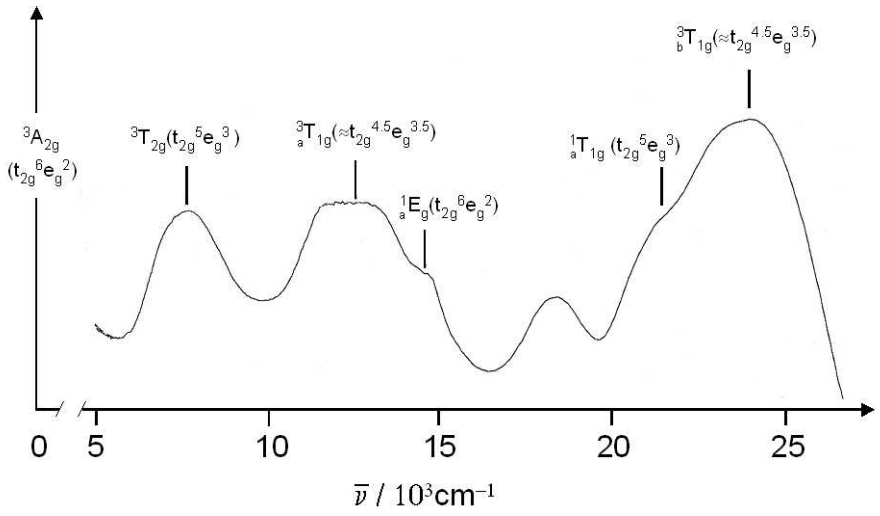

275x190mm (96 x 96 DPI)

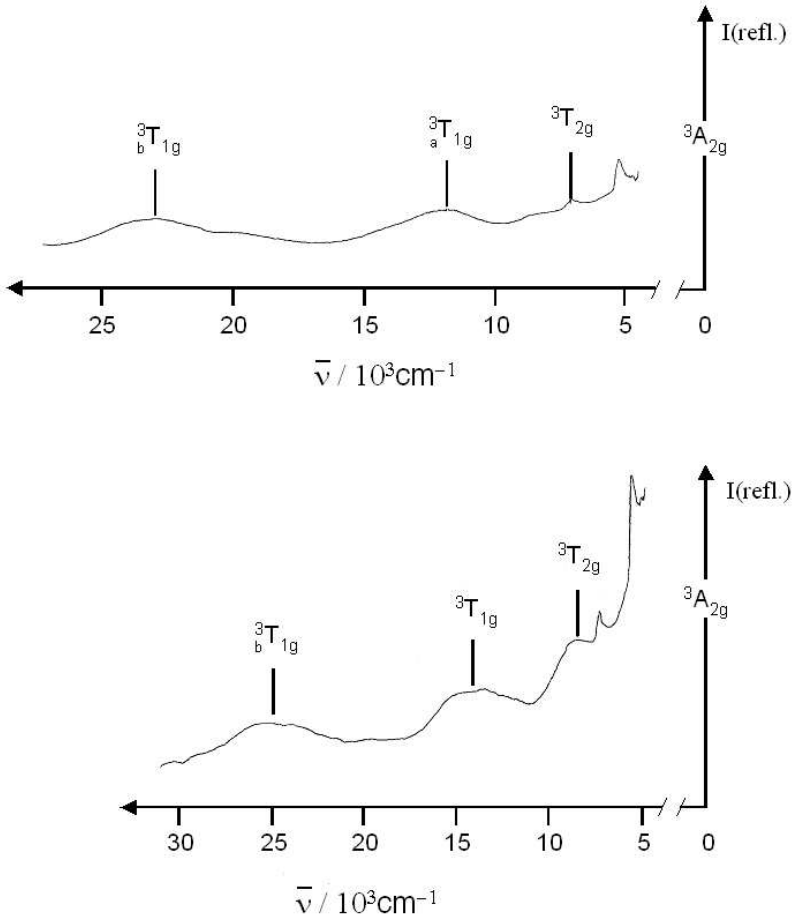

190x275mm (96 x 96 DPI)

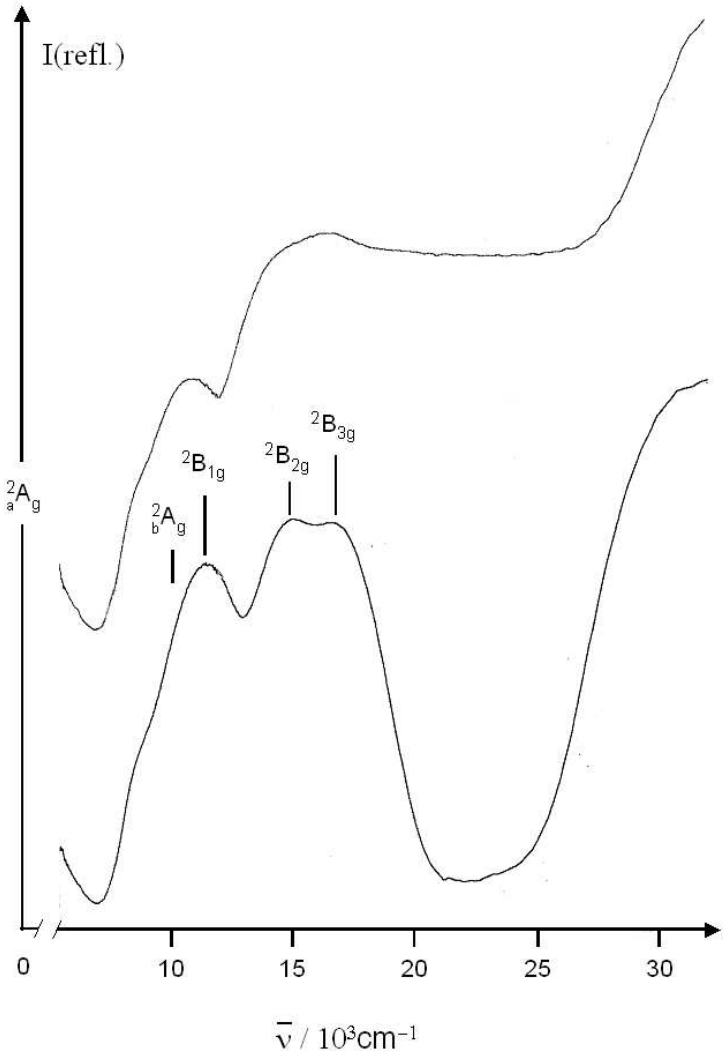

190x275mm (96 x 96 DPI)

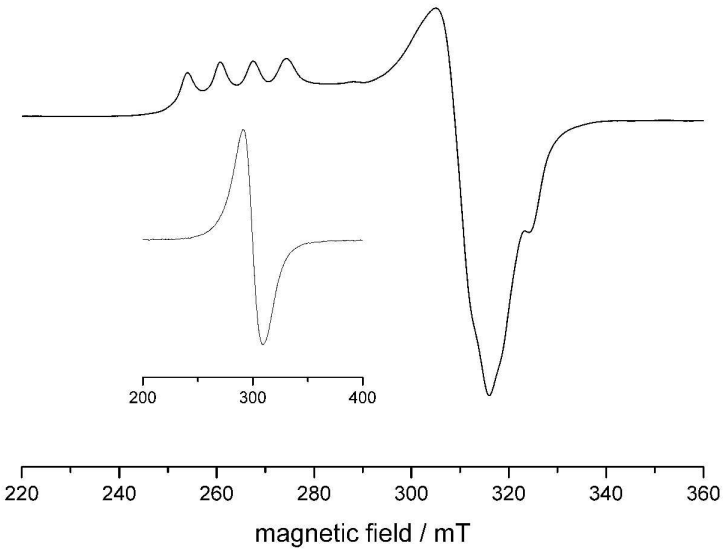

281x203mm (600 x 600 DPI)

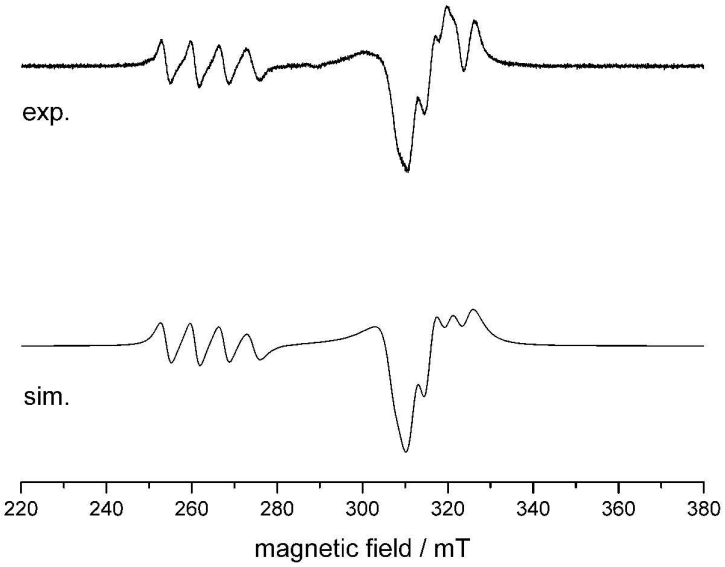

281x203mm (600 x 600 DPI)

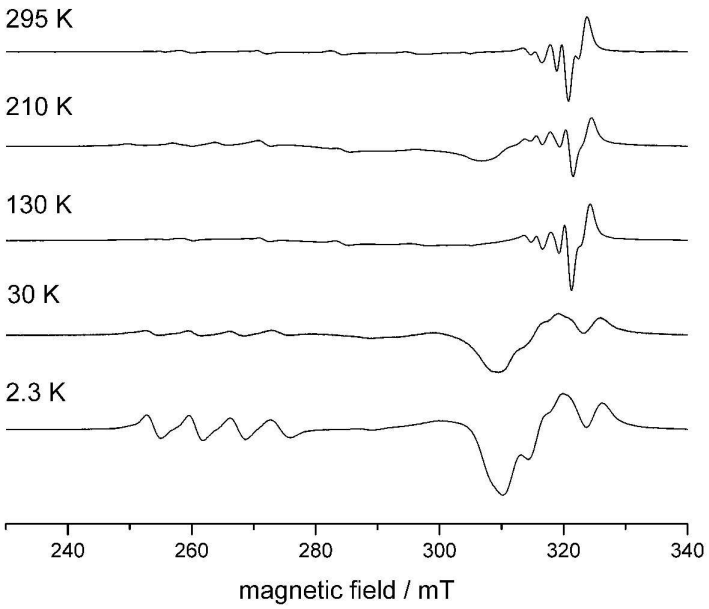

281x203mm (600 x 600 DPI)

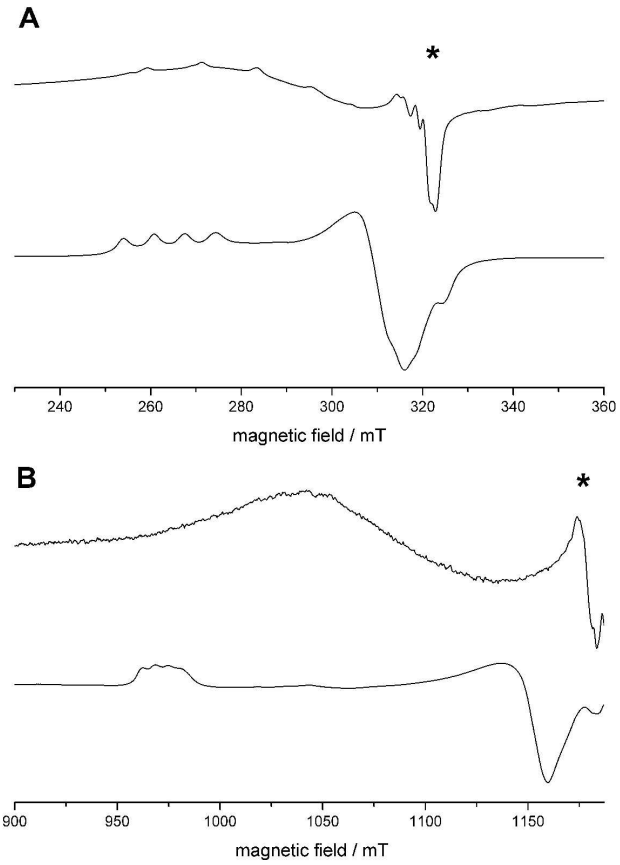

203x281mm (600 x 600 DPI)